Fuel 308 (2022) 121900

Contents lists available at ScienceDirect

Fuel

journal homepage: www.elsevier.com/locate/fuel

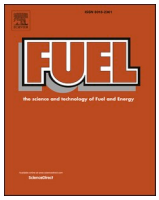

Full Length Article

Enhancing pyrolysis gas and bio-oil formation through transition metals as *in situ* catalysts

Andrew H. Hubble [a,*], Emily M. Ryan [b], Jillian L. Goldfarb [a]

[a] Department of Biological and Environmental Engineering, Cornell University, Ithaca, NY 14853, USA
[b] Department of Mechanical Engineering, Division of Materials Science & Engineering, Boston University, Boston, MA 02215, USA

ARTICLE INFO

Keywords:
Pyrolysis
Catalysts
Transition metals
Nickel
Copper
Cellulose

ABSTRACT

Biobased fuels resulting from the pyrolysis of lignocellulosic materials suffer from several key issues. Only a portion of the biomass feedstock is converted to pyrolysis oil, and only a portion of compounds in that oil represent desired end products. Bio-oil contains myriad oxygenated and aromatic compounds, many of which form tars and impart high acidity, viscosity, and instability. This necessitates substantial upgrading to generate a stable, valuable product. The inclusion of *in situ* catalysts during pyrolysis can improve the pyrolysis oil by promoting the cracking of tarry compounds and formation of smaller furans and phenols. This study examines the impact of *in situ* transition metal catalysts on cellulose pyrolysis, quantifying changes in bio-oil composition and non-condensable gas generation. Cellulose was wet impregnated with six different metal acetates at a concentration of 0.05 M and pyrolyzed at 600 °C, and some samples additionally pyrolyzed at 350 °C. The metals enhanced devolatilization, increasing hydrogen gas production at high and low temperatures and improved bio-oil yields while decreasing the average molecular weight of the oil compounds. Nickel proved to be the most effective at generating hydrogen gas and producing a wider array of light-weight bio-oil compounds. Copper aided dehydrogenation at lower temperatures and began the initial stages of primary pyrolysis by generating levoglucosenone and glucopyranose. These findings shed light on metal-biomass interactions and contribute to the growing body of knowledge of *in situ* bio-oil upgrading. By understanding how catalysts improve bio-oils we can generate high-density and cleaner-burning liquid fuels to displace the use of fossil fuels.

1. Introduction

The efficient conversion of waste biomass to renewable liquid and gaseous fuels is a longstanding goal of myriad global efforts to mitigate the anthropogenic impacts of climate change via sustainable energy generation [1]. One current thermochemical valorization scheme, pyrolysis (devolatilization at high temperatures under an inert atmosphere), generates biochar, non-condensable gases (e.g. hydrogen, carbon monoxide and low molecular weight hydrocarbons), and liquid bio-oils, all potential substitutes for fossil fuels. Pyrolysis is one of the oldest and simplest thermochemical conversion processes. However widespread application is stunted due to issues stemming both from the biomass feedstock itself, and the high input-energy nature of pyrolysis [2–5]. Pyrolysis is a non-targeted process, producing a liquid bio-oil product comprised of a single compound is nearly impossible [6–7]. The goal, therefore, is to reduce the number of undesirable products produced, especially in the liquid phase. This requires suppressing oxygenated and large tar compounds and promoting the formation of smaller furans and phenols [8–10].

The Renewable Fuels literature is replete with explorations of pyrolysis bio-oil upgrading through chemical and thermal means, such as high pressure and catalytic transformations [11–13]. These catalysts are often used downstream in a fixed/fluidized bed over which products pass. For example, second-generation cellulosic biofuels, such as those from agricultural residues, are improved by nanoparticles such as ruthenium-based catalysts to increase yields of hexitol, sorbitol and isosorbide, and tungsten-based catalysts for improving ethylene glycol production, and metal formates to improve catechol [14–17]. When included during pyrolysis, catalysts have the ability to promote the devolatilization of biomass and help reduce larger compounds to smaller, more desirable ones [18–21]. Additionally, catalysts can lower reaction pathways' activation energy; reducing the energy demand for the conversion process helps make the system more energy efficient [22]. Among the array of potential catalysts, transition metals are

* Corresponding author.
E-mail address: ahh92@cornell.edu (A.H. Hubble).

https://doi.org/10.1016/j.fuel.2021.121900
Received 14 June 2021; Received in revised form 29 August 2021; Accepted 1 September 2021
Available online 17 September 2021
0016-2361/© 2021 Elsevier Ltd. All rights reserved.

attractive options as they are relatively inexpensive and useable in many forms when compared to other pre-formed catalysts [23–24]. When used *in situ*, rather than as a separate downstream upgrading step to improve products after formation, metal catalysts can steer product formation in real-time.

Previous experimentation with *in situ* transition metal catalysts utilized chromium(III) in a closed heated batch container to enhance the conversion of glucose to 5-Hydroxymethylfurfural (HMF) [25] – a desirable biorefinery feedstock, which can be readily converted into petrochemical end products [26]. Bali achieved HMF yields of over 70%. This high conversion rate was achieved through a mechanism whereby glucose coordinates to the active metal species – the chromium (III) – in the presence of 1-ethyl-3-methylimidazolium chloride ionic liquid. Glucose then undergoes mutarotation to the β-glucopyranose anomer, and finally forms HMF. The effectiveness of chromium (III) is likely due to the low substitution rate across the first row of transition metals. The low substitution is caused by the high crystal-field stabilization energy of the ion forms, resulting in high activation energies required to achieve reaction intermediaries [25,27].

Additionally, similar work using sulfated metal oxides has shown transition metals to be effective catalysts. The duality of containing both Lewis and Brønsted acid sites is likely the root of the enhanced catalytic activity [28]. These acid sites produce an activated complex with the biomass and form carbocations during initiation, and continue throughout the chain propagation phase [29]. Each broken C–C bond has the potential to generate a new carbenium ion, which can desorb and form alkenes or alkanes, or interact with the reactant [30]. Shao et al. utilized sulfated TiO_2 nanosheets to bolster the conversion of fructose to ethyl levulinate in ethanol and fructose to HMF in dimethyl sulfoxide [31]. Lu et al. found high rates of oligomer and primary pyrolysis product reduction, and increases in light furans when reacting cellulose with SnO_2 and ZrO2 [32].

The existing literature has investigated a handful of metal catalysts used in conjunction with biomass undergoing thermochemical conversion, however not all possible metal catalysts have been investigated, and no unifying understanding yet exits. The knowledge of these discrete studies is not yet full enough to develop a general understanding of how metals affect biomass during thermochemical conversion. Additionally, many common and potentially useful transition metals have been excluded from consideration. This work identifies a wider array of potential transition metal catalysts that positively impact the pyrolysis of cellulose. The use of transition metals as *in situ* catalysts reduces the number of downstream upgrading steps and reduces the energy input required to form the end product. Additionally, if common and inexpensive transition metal catalysts can be identified as effective catalysts, the need to recharge and recycle the metals is not as great. Cellulose, used as a model biomass compound, is one of the most abundant biopolymers, whose properties have been well researched and are understood. A pyrolysis temperature of 600 °C and heating rate of 10 °C/min were selected due to the large body of existing literature at these conditions, and the high degree of biomass conversion at these conditions. The effects of transition metals on cellulose reaction rates are measured based on thermogravimetric analysis (TGA); the production of non-condensable gases analyzed via residual gas analyzer mass spectroscopy (RGA); changes in bio-oil characterized through gas chromatography-mass spectroscopy (GC–MS). By incorporating transition metals directly into cellulose pyrolysis, the aim is to: (1) reduce the formation of large tar compounds in the bio-oil, (2) increase small stable aromatic hydrocarbon production in the bio-oil, and (3) Initiate thermal degradation of cellulose at lower pyrolysis temperatures. From a fundamental standpoint, this work may open new lines of inquiry into the development of catalysts for pyrolysis biofuel upgrading by understanding key reactions promoted or curtailed by the use of transition metals. In addition, heterogeneous biochar-catalyst composites – made by pyrolyzing metal-impregnated biomass – are emerging as catalysts for downstream biorefinery applications [33], as well as functionalized adsorbents [34–36] and even support for wound dressings [37].

2. Materials and methods

Six metal acetate compounds were procured from Sigma Aldrich: Iron(II) [Cat:339199, 95%], silver [Cat:85140, ≥99%], manganese(II) [Cat:221007, ≥99%], copper(II) [Cat:341746, 98%], nickel(II) [Cat:244066, 98%], and zinc [Cat:383058, ≥98%] and were used as received. A wet impregnation method with cellulose was selected to ensure uniform distribution of metals within the biomass matrix.

Cellulose filter paper (GE Whatman Grade 40, Cat:1440-090) was soaked in 50 mL of 0.05 M metal solutions made with Milli-q water (18.2 mq·cm/25 °C) for one hour. Additionally, a blank set was introduced, where the cellulose filter paper was soaked in only the Milli-q water with no metal. Five sets of the blank and each metal-cellulose impregnation were created: one for TGA analysis (replicate 1A), and four for furnace pyrolysis (1B-1E). A hole punch was used to generate approximately 3 mg cellulose disks from the 1A replicate for TGA analysis. To ensure enough sample was available for analysis post-pyrolysis, two filter paper sheets were run simultaneously in duplicate (replicates 1B&1E and 1C&1D). Samples were dried at room temperature for three days. Both acetate and metal are adsorbed by the cellulose filter paper, and to determine the metal uptake the acetate component must be accounted for. The adjusted metal uptake on the filter papers is expressed as a percent change in Table 1.

With five filter papers of each type generated, two are paired together to ensure enough sample, and this process is repeated for a duplicate run to ensure the accuracy of measurements. Papers 'B' and 'E' are run simultaneously and are compared to papers 'C' and 'D' to confirm the accuracy of biochar, bio-oil, and pyrolysis gasses generated. Throughout this manuscript, where applicable/feasible, results are presented as the average ± one standard deviation with three or more trials, or as the average ± a percent difference between duplicate trials. TGA and proximate analysis were run as duplicates from a single filter paper ('A').

The metal uptake on cellulose filter paper represented an average 1.7% increase in mass, with all except one sample remaining within two standard deviations. The outlier, silver, can be explained: silver complexes with a single acetate, whereas the rest of the metals pair with two. Given the same uptake of mass, a greater portion remaining is silver. The blank samples showed no significant change in mass after soaking in Milli-Q water.

A second and third group of copper and nickel impregnated filter papers (and a new set of blanks) was produced after the original trials of metals in Table 1 to examine the effects of changing pyrolysis conditions on these two candidate metals. Copper and nickel were chosen for their observed ability to enhance hydrogen gas production. This set of 24 filter papers were similarly paired to pyrolyze two at the same time to give an additional 3 pyrolysis samples for each metal in duplicates. Replicates 2A&2D, 2B&2E, 2C&2F, 3A&3D, 3B&3E, and 3C&3F were pyrolyzed together. Percent change in mass from metal uptake in the second and third group are recorded in Table 2. With an average mass increase of 0.93%, these samples are lower than the first group, but remain within 2 standard deviations of each other. Group 1 reused the metal acetate solution across the 5 replicates: adding back the quantities absorbed. This required preparing samples individually, so in the interest of time, groups 2 and 3 were prepared simultaneously without reusing solution.

Group 1 (outlined in Table 1) were all subject to the same pyrolysis conditions: 10 °C/min to 600 °C for one hour, with 100 mL/min of nitrogen purge gas. Groups 2 and 3 included a mix of pyrolysis conditions, including lower final temperatures (Batch 2C&2F and 3C&3F) and higher nitrogen purge rates (Batch 2B&2E and 3B&3E). The differences in pyrolysis conditions are illustrated in Table 3.

Pyrolysis was conducted in a 2-inch diameter quartz tube furnace (MTI single heating zone GSL-1100X), with a 100 mL/min nitrogen

Table 1
Percent change of metal uptake on cellulose (by mass).

	Replicate 1A (%)	Replicate 1B (%)	Replicate 1C (%)	Replicate 1D (%)	Replicate 1E (%)	Average ± STDEV
Silver	2.9	3.3	2.5	2.8	2.9	2.9 ± 0.2
Iron(II)	2.3	1.4	1.1	1.3	1.2	1.5 ± 0.4
Copper(II)	1.7	1.4	1.1	1.2	1.1	1.3 ± 0.2
Manganese(II)	2.0	1.6	1.3	1.4	1.5	1.6 ± 0.2
Nickel(II)	1.8	1.6	1.3	1.4	1.3	1.5 ± 0.2
Zinc	2.0	1.7	1.4	1.5	1.4	1.6 ± 0.2

Table 2
Percent change of copper and nickel uptake on cellulose.

	Replicate 2A (%)	Replicate 2B (%)	Replicate 2C (%)	Replicate 2D (%)	Replicate 2E (%)	Replicate 2F (%)	Average ± STDEV
Copper(II)	0.87	0.96	0.99	0.94	0.98	0.97	0.95 ± 0.04
Nickel(II)	1.11	1.09	1.15	1.13	1.11	1.11	1.12 ± 0.02
	Replicate 3A (%)	Replicate 3B (%)	Replicate 3C (%)	Replicate 3D (%)	Replicate 3E (%)	Replicate 3F (%)	Average ± STDEV
Copper(II)	0.67	0.70	0.71	0.71	0.69	0.69	0.70 ± 0.01
Nickel(II)	0.94	0.98	1.00	0.96	0.96	0.97	0.97 ± 0.02

Table 3
Group and batch pyrolysis experimental matrix.

	Group 1	Batch 2A&2D	Batch 2B&2E	Batch 2C&2F	Batch 3A&3D	Batch 3B&3E	Batch 3C&3F
Final pyrolysis temperature (°C)	600	600	600	350	600	600	350
Nitrogen purge gas rate (mL/min)	100	100	200	100	100	200	100

purge (<0.1% O_2) from a nitrogen gas generator (Parker Balston Model N2-04), controlled with an Omega mass flow controller (FMA-5500). Batches 2B&2E and 3B&3E were run at 200 mL/min of N_2 gas to determine the effect of purge gas rate on bio-oil formation. The nitrogen purge gas flowed from the tube furnace directly into a set of two cold traps (Chemglass schwartz drying tubes) immersed in a dry ice and glycol bath to condense and collect the bio-oil. After condensation, the exhaust gas was sampled and analyzed with an RGA (residual gas analyzer, Extorr XT300M with Pfeiffer HiCube 80 Eco Vacuum) to determine the makeup of the non-condensable gas products. The RGA analyzed the non-condensable gas in real time, utilizing a 40 μm ID silica glass capillary. Mass to charge (m/z) ratios of two gases: hydrogen ($m/z = 2$) and carbon dioxide ($m/z = 44$) were monitored and are analyzed below. Due to the overlap of mass-to-charge ratios, and the high signal to noise tendency generated from the small sample sizes utilized here, other common gases were excluded from this work.

Impregnated cellulose samples were placed in a porcelain combustion boat in the furnace, and the furnace was purged with nitrogen for 10 min before starting, to allow residual oxygen to be displaced. Samples were heated at 10 °C/min to 110 °C for 30 min to drive off residual moisture before continuing up to 600 °C and holding for 60 min. Batches 2C&2F and 3C&3F were run to only 350 °C for 60 min to examine the low temperature formation of bio-oil. The furnace was cooled to 80 °C before samples could be retrieved, to ensure that the heated sample was not oxidized. The resulting biochar was weighed to determine the solid yield mass fraction, and the cold traps were weighed and rinsed with 10 mL DCM (dichloromethane) to recover the bio-oil.

Water is a byproduct of pyrolysis and must be removed from the bio-oil before analysis. The total amount of water generated during these experiments was less than 2% of the bio-oil by weight. After extraction from the cold traps, 1 mL of the DCM and bio-oil mixture was dried over approximately 0.1 g AMS (anhydrous magnesium sulfate, fisher scientific) in a 1.5 mL polypropylene centrifuge tube. The tubes were shaken by hand for four minutes and centrifuged for two minutes to bind the water and AMS and separate the solid and liquid phases so the dried oil could be recovered. Weights at each step were taken to determine the water content of the oil.

To analyze the dried bio-oil via gas chromatography-mass spectroscopy (GC–MS, Shimadzu QP2020 with AOC-20i Autosampler), the oil was further diluted in DCM. 0.2 mL dried bio-oil was mixed with 0.5 mL DCM for a total dilution ratio of approximately 40:1. The bio-oil samples were run with an initial oven temperature of 40 °C and injected at 250 °C into a Shimadzu Crossbond 30 m long 0.25 mm ID column with a split ratio of 15:1 and a helium flow of 1 mL/min. The oven was held at 40 °C for 5 min, then ramped at 5 °C/min to 150 °C and was held for an additional 5 min. The oven continued up to 250 °C at 1.75 °C/min and was held for 10 min. Ion source and interface temperatures were 230 °C and 250 °C, respectively. After a 6-minute solvent cut time, the mass spectrometer scanned from 15 to 400 m/z via electron ionization. Resulting peaks with slopes ≥900 and durations ≥1 s were identified and analyzed. Compounds were matched by spectra through an internal NIST library, with marker compounds confirmed by calibration solutions.

3. Results and discussion

3.1. Proximate and thermogravimetric analysis

Batch 1A was used to determine proximate analysis of samples after metal impregnation. While the cellulose filter paper is sold as ashless, the addition of the metal acetates introduces a small quantity of non-volatile or non-oxidizable material, as seen in Table 4. The duplicates are averaged and the percent difference between duplicate runs is given in the last column.

The largest portion of cellulose resides in the volatile matter region, with little remaining as fixed carbon, and ash attributed to the addition of the metal catalysts. This is in agreement with the body of literature surrounding the thermal degradation of cellulose [38–39].

3.2. Residual gas analysis

Non-condensable gas production (baselined to weight of input cellulose) offers insight to the impact of metal on the cellulose filter paper, as carbon dioxide and hydrogen gas are indicators of pyrolytic activity.

Table 4
Proximate analysis of metal impregnated filter papers.

	Volatile Matter [wt % dry basis]	Fixed Carbon [wt % dry basis]	Ash [wt % dry basis]	Percent Difference Between Duplicate Runs (%)*
Blank	96.43	3.43	0.14	1.13
Silver	96.05	3.01	0.95	0.83
Iron(II)	96.34	2.75	0.91	0.54
Copper(II)	97.11	2.44	0.46	0.47
Manganese(II)	93.91	5.50	0.60	0.41
Nickel(II)	98.42	0.89	0.52	0.48
Zinc	92.46	7.17	0.36	0.85

* Percent difference calculated based on mass loss during loss of volatile matter across duplicate runs.

Carbon dioxide, being a low-energy state product, confirms that the cellulose is undergoing a transformation, namely devolatilization. Cellulose depolymerizes and forms tar, char, and carbon dioxide when undergoing (initial) pyrolysis [40]. Dehydrogenation is similarly an indicator, as the formation of hydrogen gas by the scission of C–H bonds leads to increased H_2 formation while preserving C–C and C–O bonds [41–43]. Fig. 1 illustrates the carbon dioxide and hydrogen formation during group 1 pyrolysis trials (averaged duplicates), with the carbon dioxide gas evolution peaking around minute 65 (at approximately 360 °C), and hydrogen between 65 and 90 min (360–600 °C). While it takes approximately 12 min to cycle the whole volume of the furnace and tubing at 100 mL/min, gases generated from the sample are quickly

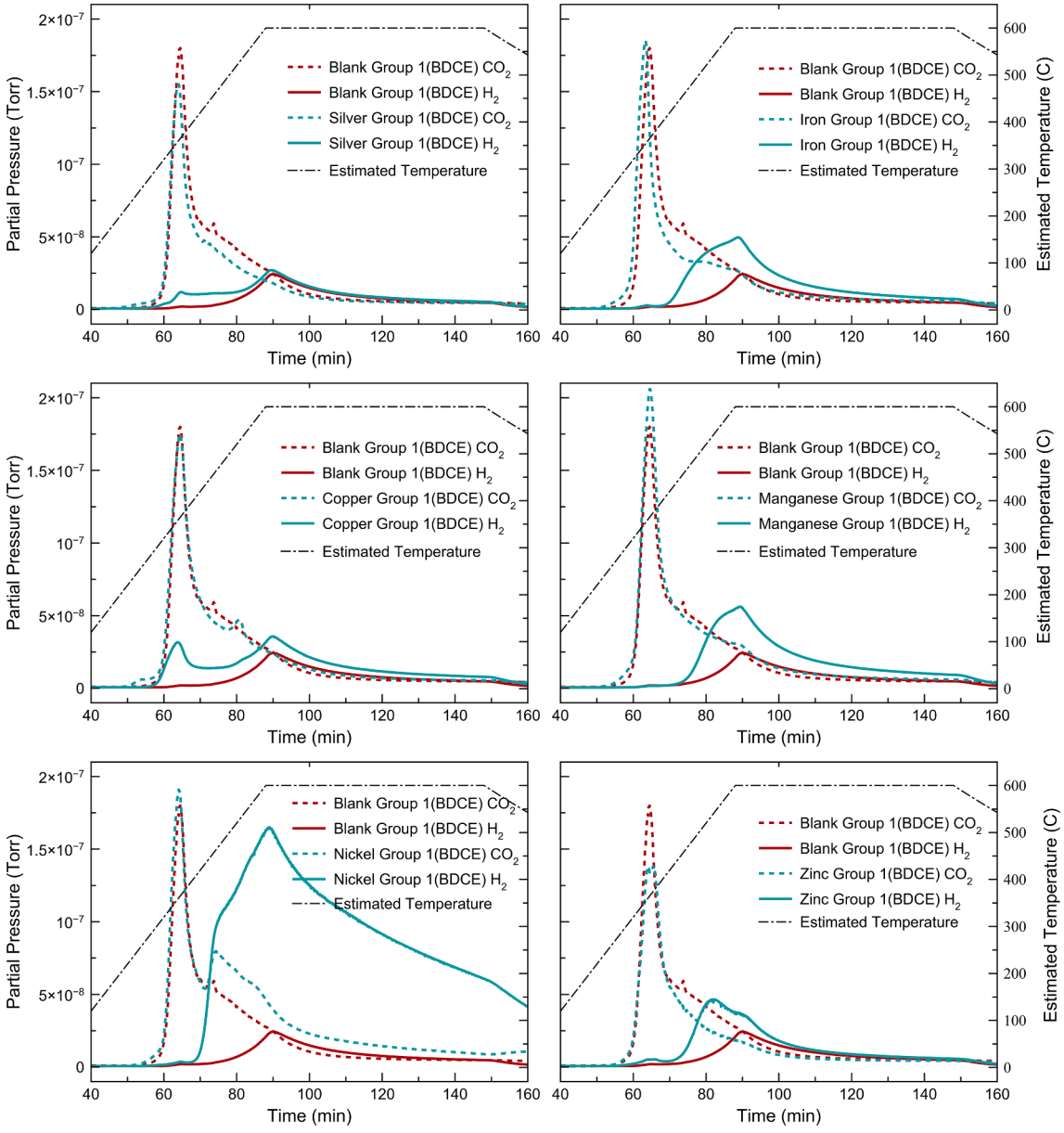

Fig. 1. Carbon dioxide (dashed) and hydrogen (solid) evolution for group 1 impregnated cellulose filter papers.

siphoned out of the furnace, and little lag is observed between generation and detection. This is confirmed by hydrogen's response to changing temperatures. For samples such as silver, copper, and nickel, as the temperature approaches 600 °C, hydrogen continues to rise. Once a steady temperature of 600 °C is reached, production begins to decrease. The temperature directly drives the hydrogen gas formation. Additionally, when the furnace begins to cool around 145 min, the hydrogen gas evolved starts to decrease faster. Were there a significant lag in response and temperature, there would be a corresponding gap in these peaks. The pyrolysis method for each sample in group 1 is the same, with only the metal differentiating the samples. While manganese peaks high and early – when compared to zinc's lower and later production, the differences between same-metal duplicates help highlight the inherent variability. Copper and nickel each produce an additional CO_2 peak between 75 and 85 min (470–570 °C).

Fig. 1 also highlights hydrogen gas production for group 1 where again copper and nickel are noted to significantly influence gas production. Nickel produced on average 934% (851.1% and 1017.6% over two runs; data in SI) more hydrogen gas than then blank no-metal baseline. Conversely, while copper produces a comparatively modest 90% (87.6% and 92.5% over two runs; data in SI) increase, a large portion of that production occurs earlier during the pyrolysis process: between 60 and 65 min (320–370 °C). This low temperature production may potentially lead to a more efficient thermochemical conversion scheme by reducing processing temperature and therefore energy requirements.

Fig. 2 highlights methane and ethane production. The inclusion of metals decreased methane production in all cases except for copper, where it was marginally increased. This trend of decreasing methane production leads to a less energy-dense pyrolysis gas (which could be combusted to offset the heating demands of the furnace). A decrease in methane – and gaseous hydrocarbons in general – equates to increased carbon and hydrogen remining in the biochar and/or bio-oil. Where a less oxygenated bio-oil is desired, this increase in carbon and hydrogen favorably improves the carbon/oxygen ratio of the bio-oil. The quantity of ethane produced saw little change over all trials, however, copper, manganese and nickel saw slightly earlier formation. This trend to form more ethane at slightly lower temperatures potentially hints at reduced barriers to conversion. Further exploration to strengthen this correlation is required before making definitive assertions.

Because copper and nickel showed considerably higher gas evolution than the other metals investigated, both were repeated in experimental groups 2 and 3 with lower final pyrolysis temperatures (350 °C reduced from 600 °C) and higher purge gas sweep rates (200 mL/min up from 100 mL/min) to confirm the low temperature production and to determine the extent of tar recondensation on the biochar. Fig. 3 depicts the hydrogen gas evolution over the three conditions (average of duplicates presented here). Batches 2 and 3 AD (solid lines) were pyrolyzed at the

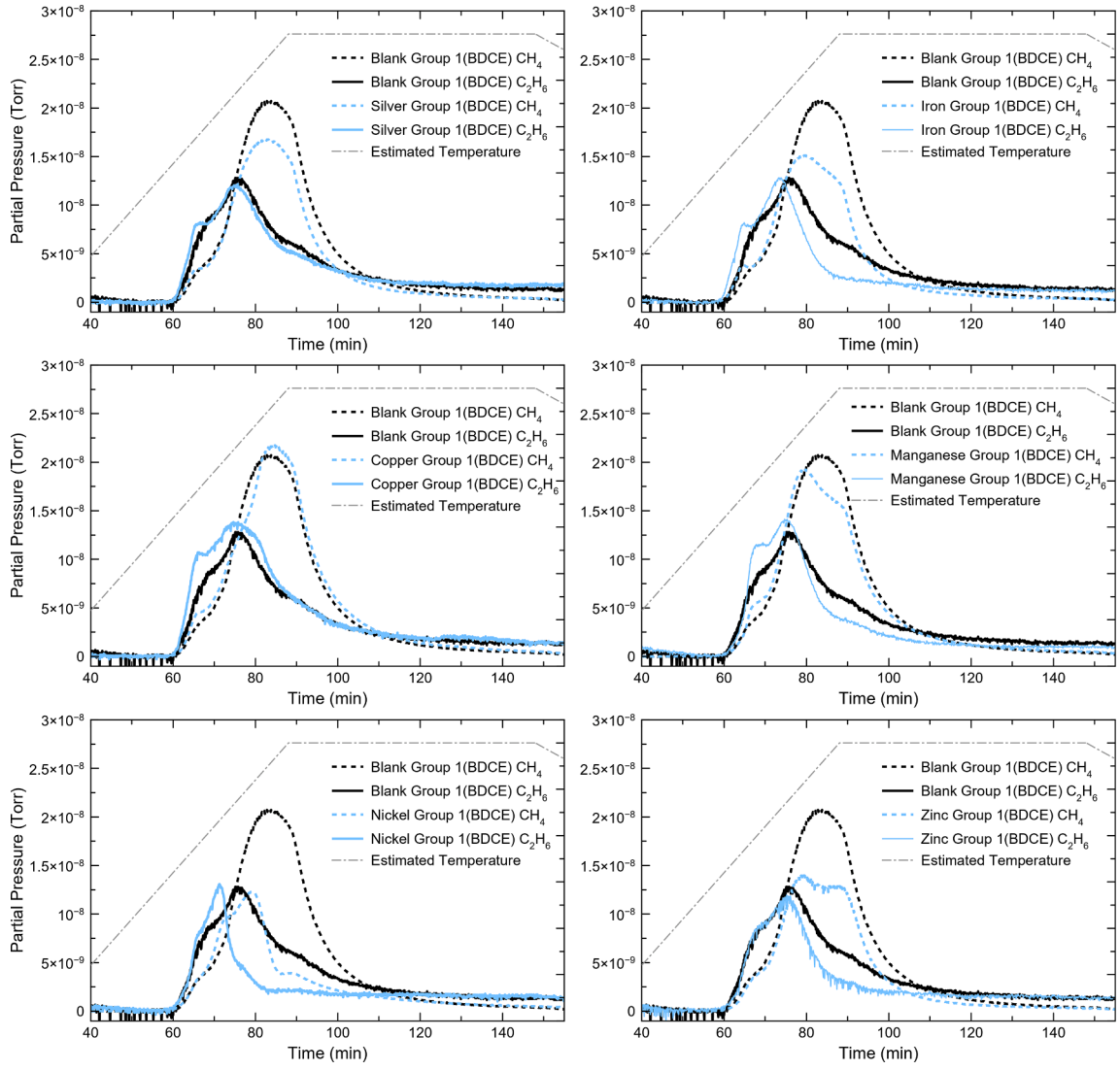

Fig. 2. Methane (dashed) and ethane (solid) evolution for group 1 impregnated cellulose filter papers.

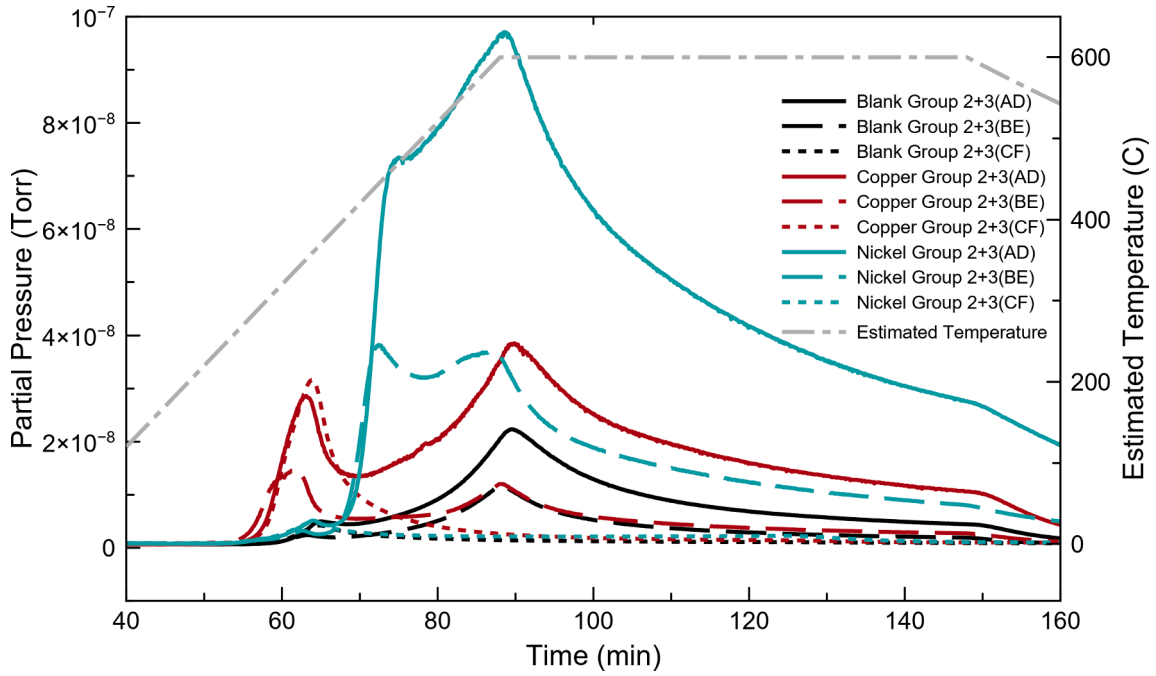

Fig. 3. Averaged hydrogen gas evolution for batches 2 and 3 impregnated cellulose filter papers.

same conditions as group 1 (600 °C with 100 mL/min N_2 purge). Nickel again produced a larger quantity of hydrogen over the no-metal baseline, increasing hydrogen production 328% (287.7% and 368.4% over two runs; data in SI) over the pure cellulose trial. Although not as high as group 1, this could potentially be attributed to the lower ratio of metal to cellulose. Copper's batch 3A&3D additionally produced more hydrogen when compared to 2A&2D, although crucially both still contain the early peak between 60 and 65 min (320–370 °C). The low temperature trials of 2C&2F and 3C&3F (peak temperature of 350 °C) produced the same quantity of hydrogen between 55 and 70 min as 2A&2D and 3A&3D (peak temperature of 600 °C), confirming copper's ability to catalyze thermochemical conversion at lower temperatures. This is highlighted by the fact that the no-metal baseline cellulose pyrolysis yields approximately 1/10th of the hydrogen over the same range. The high sweep rate of 200 mL/min for batches 2B&2E and 3B&3E produces a lower hydrogen signal, but it is important to remember that this hydrogen is diluted in twice the nitrogen. If corrected for the increased dilution, copper and nickel effectively generated the same quantity of hydrogen, differentiating by 0.18% and 0.31% respectively. Copper and nickel's carbon dioxide differed by 0.04% and 0.25% respectively. Increasing the sweep gas rate had no significant effect on the gases generated.

Repeating the group 1 experiments and focusing in on copper and nickel at varying purge rates and temperatures indicates the robustness of these findings. Nickel is effectively catalyzing the transition of cellulose at higher temperatures, and copper at lower temperatures. While hydrogen is a good indicator of activity, the bio-oil requires closer examination to determine the extent of these effects on the pyrolysis process.

3.3. Gas chromatography mass spectroscopy analysis of pyrolysis bio-oil

Bio-oil quantities across samples were normalized to the input mass of cellulose. Table 5 shows average biochar, bio-oil, and bio-oil water (limited to trials with final temperatures of 600 °C) with standard deviations for the control, nickel, and copper which were run six times over the two groups at the 600 °C condition. Percent difference is reported for the remaining values which were run twice. As we can see, the increase in bio-oil yield for the copper and nickel versus the pure cellulose are not statistically significant.

The remaining metals were run twice each (in group 1), and as a result have too few data points to accurately draw conclusions. Copper, nickel, and the control however were each run six times over the three groups (excluding the two low temperature batches 2C&2F and 3C&3F where little oil is generated).

Most of the metal catalyst biochar yields increase slightly over the control. These values are reported on a pure-biomass basis and discount the addition of the metals which would further increase the weight of the remaining biochar. An increase in biochar weight could be an indicator of decreased primary devolatilization, or a tendency to favor the recondensing of tar compounds during secondary pyrolysis. Because the bio-oil yields are mixed – some higher than the blank and some lower –

Table 5
Average biochar, bio-oil, and bio-oil water yields at 600 °C (±one standard deviation where n > 2, otherwise error reported as percent difference between duplicate trials.)

	Average biochar yield (% wt)	Average bio-oil yield (% wt)	Average bio-oil water content (% wt)
Blank (no-metal)	12.43 ± 0.55	73.8 ± 11.7	1.54 ± 0.47
Copper	14.14 ± 0.91	78.3 ± 10.1	1.27 ± 0.55
Nickel	9.45 ± 1.68	71.0 ± 11.4	1.60 ± 1.16
Silver	13.14 (18.2%)	81.0 (18.8%)	2.11 (37.0%)
Iron	15.13 (2.6%)	76.1 (26.4%)	3.23 (23.3%)
Manganese	15.26 (0.4%)	81.3 (17.4%)	2.84 (28.2%)
Zinc	16.68 (0.5%)	62.9 (33.6%)	3.32 (33.7%)

Table 6
Group 1 bio-oil compound yields expressed as percent change in chromatogram area versus pure cellulose (negative indicates decrease in yield versus cellulose).

	MW (g/mol)	Silver (%)	Iron (II) (%)	Copper (II) (%)	Manganese (II) (%)	Nickel (II) (%)	Zinc (%)
Furfural	96.08	−27.6	−11.4	−40.5	−9.3	25.4	60.8
2-Propyl Furan	110.15	−14.1	−55.6	−2.8	−61.4	−20.4	−43.8
2(5H)-Furanone	84.07	−0.4	−47.2	−37.7	49.3	19.4	16.5
1-(2-furanyl)-Ethanone	110.11	35.3	−13.5	19.0	−31.7	−2.7	−16.0
3-Hydroxy-2(1H)-Pyridinone	111.10	−48.6	53.9	−38.9	148.2	563.4	−15.0
5-methyl-2-Furancarboxaldehyde	110.11	−26.6	55.9	−31.2	43.1	144.2	151.8
Phenol	94.11	1.4	−28.8	−17.2	−17.6	−13.1	−2.4
3-methyl-1,2-Cyclopentanedione	112.13	−10.3	94.1	8.5	46.7	78.0	23.6
Levoglucosenone	126.11	34.0	−37.3	57.4	−38.4	−1.0	14.3
Heptanal	114.19	−62.2	78.9	−61.8	49.3	190.1	446.8
1,4:3,6-Dianhydro-α-d-glucopyranose	144.13	−8.0	−24.7	−2.9	−20.3	−16.9	6.7
1,6-anhydro-β-D-Glucopyranose	162.14	11.3	23.7	−31.6	36.9	−37.4	−44.5

there is no blanket consensus on whether the initial devolatilization is significantly affected since there should be an increase in either the oil or gas phases. Instead, if the metals favor tar depositing back on the biochar surface, then a corresponding decrease in tar compounds in the oil would be expected.

The water content of the bio-oils is similarly mixed. Water is an expected byproduct of the pyrolysis process, and with an oxygen-deficient atmosphere, the formation of water requires the oxygen to be sourced from the biomass itself (in an otherwise dry nitrogen purge stream). An increase in bio-oil water potentially leads to fewer oxygenated compounds in the gas stream, or fewer oxygenated bio-oil compounds. One of the primary ways oxygen leaves through the gas phase is via CO and CO_2. A reduction in oxygen here would correlate to a reduction in carbon. This carbon, when retained in the oil or char, represent an increase in available energy-valuable bonds. A reduction in oxygen in the bio-oil compounds is an improvement, as fewer oxygen atoms equates to an increase in energy density, decreases instability, and reduces acidity. High water contents in the oil however present a problem at scale. Water must be removed before the bio-oil can be stored or used.

Table 6 highlights the 11 most prominent bio-oil compounds identified in each sample from group 1 and are represented as a percent change from the baseline (no-metal) cellulose blank. The duplicate runs were averaged to incorporate both sets of data. The individual percent change data can be found in SI. In general, desirable light compounds elute at lower retention times, and are therefore at the top of the table. Heavier tar compounds (Italicized) are seen in the latter half of the table, with the notable exception of heptanal, which while containing an alcohol group, is not nearly as oxygenated as others around it.

Many of the changes to the bio-oil are subtle or lateral – with compounds often being replaced by isomers or congeners. Pure cellulose

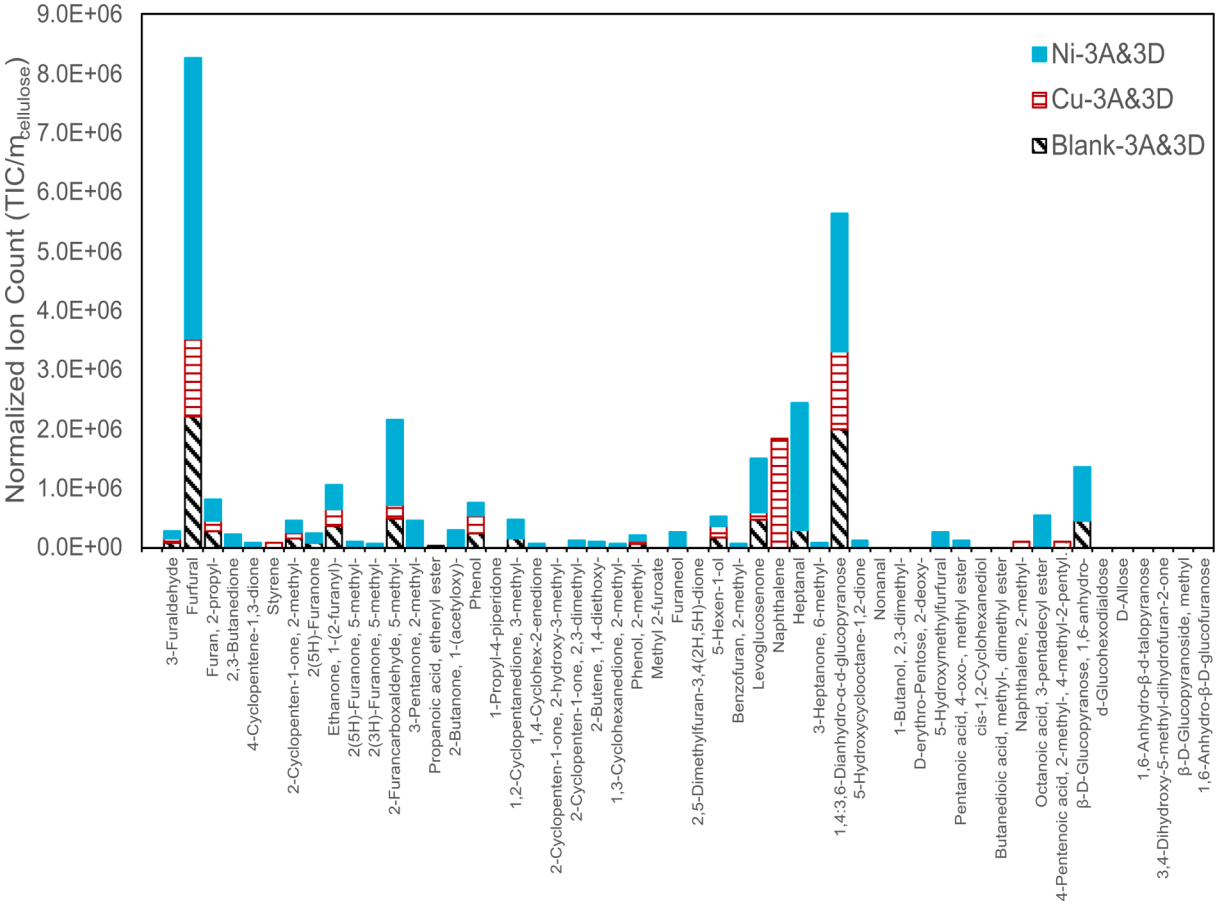

Fig. 4. Bio-oil compound distribution normalized to mass of input cellulose at 600 °C and 100 mL/min.

generates a significant quantity of furfural, which is used in industry as a feedstock to generate other furan derivatives [44]. Furfural – and other light compounds – decreased in prominence with the addition of most metals. Notable exceptions to this are nickel, copper, and zinc.

Nickel bolstered the formation of furfural, 3-hydroxy-2(1H)-pyridinone, 5-methyl-2-furancarboxaldehyde, and heptanal. These four compounds already represent a major fraction of the bio-oil composition, and if isolation of these potential biorefinery feedstock compounds is desired, the addition of nickel would represent a major improvement in yields. In addition, nickel decreased the large undesirable tar compounds levoglucosenone, 1,4:3,6-Dianhydro-α-d-glucopyranose, and 1,6-anhydro-β-D-Glucopyranose, which are contributors to bio-oil's generally high viscosity and acidity and low stability [45]. Zinc had a similar effect on the bio-oil as nickel, increasing furfural and heptanal, and decreasing some tar formation (1,6-anhydro-β-D-Glucopyranose), although not to the same degree as nickel. Copper, despite the early low-temperature dehydrogenation, increased the quantity of levoglucosenone – a preliminary pyrolysis product indicative of activity, but an undesirable end-product. This makes copper appear undesirable as a catalyst, however given copper's activity at low temperature, group 2 and 3 bio-oil must be examined for a direct comparison.

Fig. 4 illustrates the compound distribution for groups 2 and 3 at 600 °C, 100 mL/min copper and nickel trials. Looking at large-scale change between these trials, nickel produces a wider array of products (and often in higher quantities) at all retention times. Light aromatics tend to appear at low retention times, with larger undesirable tar compounds eluting at higher retention times. This indicates that nickel's ability to spur thermal degradation is not limited to any singular region, nor is it likely to be selective during primary or secondary pyrolysis. Nickel enhances the conversion of biomass into oil and gas products, as confirmed by lower amounts of remaining biochar for both high temperature (A&D and B&E) reactions, seen in Table 5.

The surface of nickel metal provides a nucleation point for the adsorption and activation of hydrogen, furans, and phenols. This allows the nickel to promote saturation of carbon–carbon double bonds, and assists in the scission of C-O bonds [46]. One of the most efficient methods to form this carbon–carbon bonding is via oxidative cyclization. The nickel likely forms organonickel complexes when reacted with carbon monoxide – a gas produced in abundance during low-oxygen thermal degradation reactions. Organonickel complexes then promote a Pauson-Kahnd reaction: a cycloaddition of alkyne, alkene, and carbon monoxide, forming cyclopentenone derivatives [47]. The effect of nickel on biomass undergoing various thermal degradation schemes has been well studied, however, its role in specific pathways is not as easily identified. This is in part due to its wide effect over the course of thermal degradation, but also the inherent difficulties in isolating the specific pathways themselves [24,48].

Fig. 5 highlights the product distribution for groups 2 and 3 at 600 °C and 200 mL/min of copper and nickel. At higher flow rates, vapors and suspended particulates have little time to react at high temperatures (both heterogeneously at the biochar surface and homogeneously in the gas phase) before being swept from the furnace. With the lower residence time, it might be assumed that nickel and copper would not have ample time to promote reactions, however, nickel produced increased quantities of lower weight aromatics at early residence times, and partially suppressed large heavy weight compounds. An increased flow rate likely prevents recondensation of compounds onto the solid biochar surface, and time-limits heterogeneous gas-char reactions. Copper saw a reduction in the tracked compounds across the board, with a few exceptions. Coupled with no observable drop in total oil yield, this indicated that copper promoted a wider array of compounds at lower concentrations. Peaks between retention times of 23–30 min

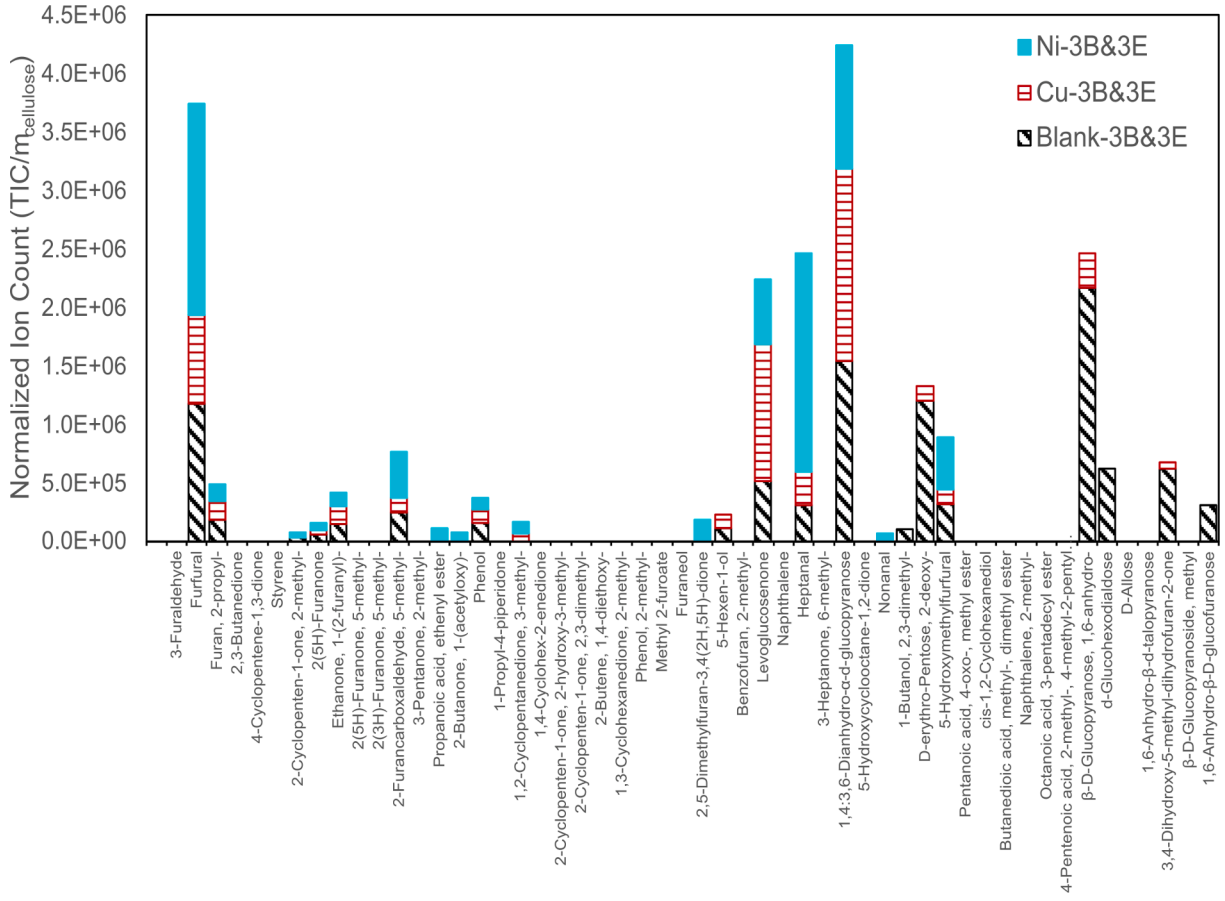

Fig. 5. Bio-oil compound distribution normalized to mass of input cellulose at 600 °C and 200 mL/min.

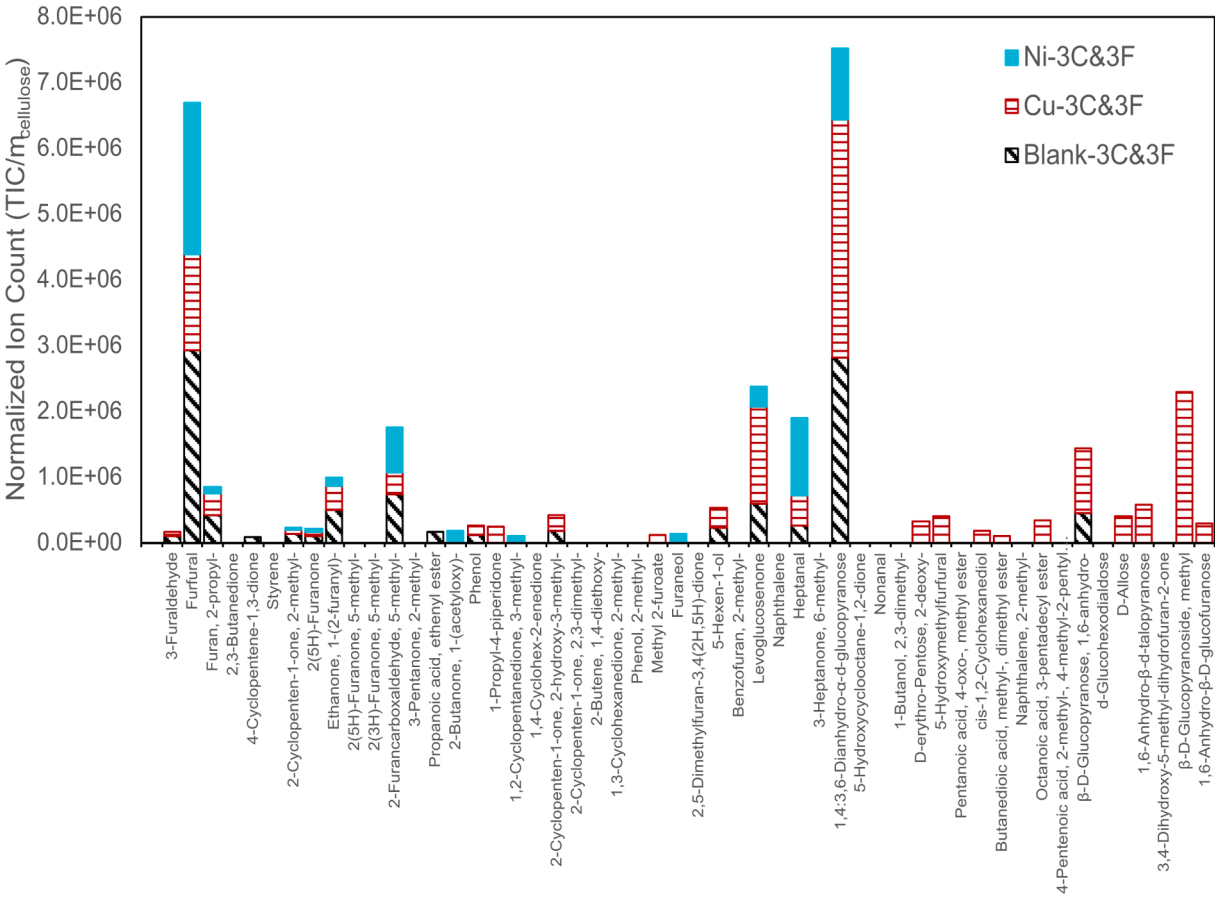

Fig. 6. Bio-oil compound distribution normalized to mass of input cellulose at 350 °C and 100 mL/min.

(corresponding to 5-hexanol, levoglucosenone, heptanal, and 1,4:3,6-Dianhydro-α-d-glucopyranose respectively) saw increases against the baseline. Levoglucosenone and 1,4:3,6-Dianhydro-α-d-glucopyranose are undesirable tar compounds. They represent the first wave of thermal degradation of cellulose and are highly oxygenated and acidic [45]. Closing the mass-balance on bio-oil production becomes progressively more difficult when the products become increasingly diverse. A reduction in observed compounds without a drop in oil yield indicates that a greater number of compounds are produced that do not meet the minimum criteria for detection. This still agrees with copper's ability to break down undesirable tar compounds, but it produces a wider array of new products, instead of generating a homogeneous oil. While at these flow rates copper doesn't produce the desired end-products, copper is still promoting the first wave of degradation from cellulose to these primary products.

Fig. 6 illustrates copper and nickel at low temperatures: 350 °C and 100 mL/min N_2 flow rate. Without the benefit of high temperatures to activate the devolatilization of cellulose, a catalyst is required. Copper produces the greatest quantity of the large tar compounds, however, while this does not represent an ideal end feedstock, it is an indicator of copper's effectiveness to promote certain reactions. Coupled with the increase in hydrogen gas production, copper is promoting the conversion of cellulose into the first set of intermediaries – known as the initiation of pyrolysis – where free radical formation is facilitated by inorganic impurities [49]. However, without the benefit of the final high temperatures, these reactions cannot be carried to completion.

Since the number of reaction pathways in the thermal degradation of lignocellulosic is high, it's not realistic to assume a single catalyst will be effective at each step. If paired with the right co– catalyst(s) that could take copper's intermediaries and convert them to the final desired products, copper could still play an important role in producing quality bio-oil at potentially lower temperatures.

In situ copper and nickel promote thermal degradation of cellulose during pyrolysis. Nickel's ability to increase the variety and quantity of bio-oil compounds, and copper's ability to promote early reactions at lower temperatures make both these metals important options for bio-oil upgrading. The formation of organonickel complexes, such as nickelacycles, are important vehicles for the transformation of organics through carbon–carbon bond formation and carbon–oxygen scission [47]. Meanwhile, copper's variable oxidation states [Cu(0), Cu(I), Cu(II), Cu(III)] allow it to effectively catalyze single and double electron pathway reactions, and its ability to pi-bond can activate terminal alkynes. Copper's affinity to promote click chemistry and carbonylation make it an invaluable tool for improving thermochemical reactions. Future research will investigate complimentary bimetal catalysts, where the beneficial effects of multiple metals could be combined to further improve bio-oil quality.

4. Conclusions

This study examines the effects of six pure transition metal catalysts under various pyrolysis conditions to study the products generated and gauge the potential for *in situ* upgrading. The current body of literature presents a narrow scope of specific catalyst-biomass interactions for a limited set of metals. The present work, probing the impacts of six transition metal catalysts, identifies nickel as effective in promoting dehydrogenation and increasing the variety of smaller aromatics while decreasing tar compounds. Copper demonstrates a strong affinity for

promoting devolatilization at lower temperature ranges (identified here as 350 °C compared to the oft-cited 600 °C) to produce larger quantities of the first-stage pyrolysis products. While the addition of copper or nickel alone does not decrease the tar and oxygenated compounds enough to compete with current fossil fuels, this first step potentially decreases the energy barriers – and shapes the pathways – for a more effective biomass to bio-oil conversion.

CRediT authorship contribution statement

Andrew H. Hubble: Conceptualization, Methodology, Investigation, Writing – original draft. **Emily M. Ryan:** Conceptualization, Writing - review & editing, Funding acquisition. **Jillian L. Goldfarb:** Conceptualization, Resources, Funding acquisition, Supervision.

Declaration of Competing Interest

The authors declare that they have no known competing financial interests or personal relationships that could have appeared to influence the work reported in this paper.

Acknowledgements

This work was supported by the National Science Foundation under grant number 1933071 and funding from the President's Council of Cornell Women.

Appendix A. Supplementary data

Supplementary data to this article can be found online at https://doi.org/10.1016/j.fuel.2021.121900.

References

[1] Basu P. Biomass gasification and pyrolysis. Comprehensive Renewable Energy 5, (Elsevier, 2012).
[2] Bridgwater AV, Peacocke GVC. Fast pyrolysis processes for Biomass. Renew Sustain Energy Rev 2000;4:1–73.
[3] Czernik S, Bridgwater AV. Overview of applications of biomass fast pyrolysis oil. Energy Fuels 2004;18(2):590–8.
[4] Bridgwater AV. Review of fast pyrolysis of biomass and product upgrading. Biomass Bioenergy 2012;38:68–94.
[5] Krutof A, Hawboldt KA. Thermodynamic model of fast pyrolysis bio-oil advanced distillation curves. Fuel 2020;261:116446. https://doi.org/10.1016/j.fuel.2019.116446.
[6] Shahbaz M. et al. Investigation of biomass components on the slow pyrolysis products yield using Aspen Plus for techno-economic analysis. Biomass Convers. Biorefinery 1–13 (2020). doi:10.1007/s13399-020-01040-1.
[7] Bridgwater AV, Meier D, Radlein D. An overview of fast pyrolysis of biomass. Org Geochem 1999;30:1479–93.
[8] Islam MW. A review of dolomite catalyst for biomass gasification tar removal. Fuel 2020;267:117095. https://doi.org/10.1016/j.fuel.2020.117095.
[9] Yi W, Wang X, Zeng K, Yang H, Shao J, Zhang S, et al. Improving bio-oil stability by fractional condensation and solvent addition. Fuel 2021;290:119929. https://doi.org/10.1016/j.fuel.2020.119929.
[10] Kaewpanha M, et al. Steam reforming of tar derived from the steam pyrolysis of biomass over metal catalyst supported on zeolite. J Taiwan Inst Chem Eng 2013;44:1022–6.
[11] Agarwal A, Park S-J, Park J-H. Catalytic upgrading of Kraft lignin derived bio-oil in supercritical ethanol over different crystal size hierarchical nano-HZSM5. Fuel 2020;271:117630. https://doi.org/10.1016/j.fuel.2020.117630.
[12] Adjaye JD, Bakhshi NN. Production of hydrocarbons by catalytic upgrading of a fast Part II : Comparative catalyst performance and reaction pathways. Fuel Process Technol 1995;45:185–202.
[13] Wang L, Xiao F. Nanoporous catalysts for biomass conversion. Green Chem 2015;17:24–39.
[14] Geboers J, Vyver SV, Van de Carpentier K. Efficient catalytic conversion of concentrated cellulose feeds to hexitols with heteropoly acids and Ru on carbon. Chem Commun 2010;46:3577–9.
[15] Deng W, Tan X, Fang W, Zhang Q, Wang Y. Conversion of cellulose into sorbitol over carbon nanotube-supported ruthenium catalyst. Catal Lett 2009;133:167–74.
[16] Wang A, Zhang T. One-pot conversion of cellulose to ethylene glycol with multifunctional tungsten-based catalysts. Acc Chem Res 2013;46:1377–86.
[17] Hashmi SF, Pitkänen L, Usvalampi A, Meriö-Talvio H, Ruuttunen K, Sixta H. Effect of metal formates on hydrothermolysis of organosolv lignin for the production of bio-oil. Fuel 2020;271:117573. https://doi.org/10.1016/j.fuel.2020.117573.
[18] Huo E, Duan D, Lei H, Liu C, Zhang Y, Wu J, et al. Phenols production form Douglas fir catalytic pyrolysis with MgO and biomass-derived activated carbon catalysts. Energy 2020;199:117459. https://doi.org/10.1016/j.energy.2020.117459.
[19] Ferreira AF, Soares Dias AP. Pyrolysis of microalgae biomass over carbonate catalysts. J Chem Technol Biotechnol 2020;95:3270–9.
[20] Ghorbannezhad P, Park S, Onwudili JA. Co-pyrolysis of biomass and plastic waste over zeolite- and sodium-based catalysts for enhanced yields of hydrocarbon products. Waste Manag 2020;102:909–18.
[21] Iisa K, French RJ, Orton KA, Dutta A, Schaidle JA. Production of low-oxygen bio-oil via ex situ catalytic fast pyrolysis and hydrotreating. Fuel 2017;207:413–22.
[22] Huber GW, Iborra S, Corma A. Synthesis of transportation fuels from biomass: Chemistry, catalysts, and engineering. Chem Rev 2006;106:4044–98.
[23] Kantarelis E, Yang W, Blasiak W. Effect of zeolite to binder ratio on product yields and composition during catalytic steam pyrolysis of biomass over transition metal modified HZSM5. Fuel 2014;122:119–25.
[24] Oyer MM, Karakaya C, Kee RJ, Rewyn BT. In situ formation of metal carbide catalysts. ChemCatChem 2017;9:3090–101.
[25] Bali S, Tofanelli MA, Ernst RD, Eyring EM. Chromium(III) catalysts in ionic liquids for the conversion of glucose to 5-(hydroxymethyl)furfural (HMF): Insight into metal catalyst:ionic liquid mediated conversion of cellulosic biomass to biofuels and chemicals. Biomass Bioenergy 2012;42:224–7.
[26] Bozell JJ, Petersen GR. Technology development for the production of biobased products from biorefinery carbohydrates—the US Department of Energy's "top 10" revisited. Green Chem. 12, 539–55 (2010).
[27] Sykes AG. Kinetics of Inorganic Reactions. Pergamon Press; 1970.
[28] Tang X, Ding W, Li H. Improved hydrodeoxygenation of bio-oil model compounds with polymethylhydrosiloxane by Brønsted acidic zeolites. Fuel 2021;290:119883. https://doi.org/10.1016/j.fuel.2020.119883.
[29] Kazansky VB, Frash MV, Van Santen RA. Quantumchemical study of the isobutane cracking on zeolites. Appl Catal A Gen 1996;146:225–47.
[30] Corma A, Orchillés AV. Current views on the mechanism of catalytic cracking. Microporous Mesoporous Mater 2000;35-36:21–30.
[31] Shao Y, et al. Sulfated TiO2 nanosheets catalyzing conversion of biomass derivatives: influences of the sulfation on distribution of Brønsted and Lewis acidic sites. J Chem Technol Biotechnol 2020;95:1337–47.
[32] Lu Q, Xiong W, Li W, Guo Q, Zhu X. Catalytic pyrolysis of cellulose with sulfated metal oxides: A promising method for obtaining high yield of light furan compounds. Bioresour Technol 2009;100:4871–6.
[33] Yu IK. et al. Aluminium-biochar composites as sustainable heterogeneous catalysts for glucose isomerisation in a biorefinery. Green Chem (2018). doi:10.1039/C8GC02466A.
[34] Liu W-J, Jiang H, Yu H-Q. Development of biochar-based functional materials: toward a sustainable platform carbon material. Chem Rev 2015;115(22):12251–85.
[35] Mullen CA, Boateng AA, Goldberg NM, Lima IM, Laird DA, Hicks KB. Bio-oil and bio-char production from corn cobs and stover by fast pyrolysis. Biomass Bioenergy 2010;34(1):67–74.
[36] Pokorna E, Postelmans N, Jenicek P, Schreurs S, Carleer R, Yperman J. Study of bio-oils and solids from flash pyrolysis of sewage sludges. Fuel 2009;88(8):1344–50.
[37] Zhou Y, Gao B, Zimmerman AR, Cao X. Biochar-supported zerovalent iron reclaims silver from aqueous solution to form antimicrobial nanocomposite. Chemosphere 2014;117:801–5.
[38] Smyth M, García A, Rader C, Foster EJ, Bras J. Extraction and process analysis of high aspect ratio cellulose nanocrystals from corn (Zea mays) agricultural residue. Ind Crops Prod 2017;108:257–66.
[39] Lazdovica K, Kampars V. Catalytic intermediate pyrolysis of cellulose for hydrocarbon production in the presence of zeolites by using tga-ftir method. *Key Engineering Materials 850 KEM*. 127–132 (Trans Tech PublicaC Ltd); 2020.
[40] Banyasz JL, Li S, Lyons-Hart J, Shafer KH. Gas evolution and the mechanism of cellulose pyrolysis. Fuel 2001;80(12):1757–63.
[41] Demirbaş A. Mechanisms of liquefaction and pyrolysis reactions of biomass. Energy Convers Manag 2000;41(6):633–46.
[42] Faix O, Jakab E, Till F, Székely T. Study on low mass thermal degradation products of milled wood lignins by thermogravimetry-mass-spectrometry. Wood Sci Technol 1988;22:323–34.
[43] Lu Q, Xie W-luan, Hu B, Liu J, Zhao W, Zhang B, et al. A novel interaction mechanism in lignin pyrolysis: Phenolics-assisted hydrogen transfer for the decomposition of the β-O-4 linkage. Combust Flame 2021;225:395–405.
[44] Hoydonckx, H. E., Van Rhijn, W. M., Van Rhijn, W., De Vos, D. E. & Jacobs, P. A. Furfural and Derivatives. in Ullmann's Encyclopedia of Industrial Chemistry (Wiley-VCH Verlag GmbH & Co. KGaA, 2007). doi:10.1002/14356007.a12_119.pub2.
[45] Blythe DA, Schroeder LR. Degradation of a nonreducing cellulose model, 1,5-anhydro-4-0-β-D-glucopyranosyl-D-glucitol, under kraft pulping conditions. J Wood Chem Technol 1985;5:313–34.
[46] Arteaga-Pérez LE, et al. Catalytic upgrading of biomass-derived vapors on carbon aerogel-supported Ni: Effect of temperature, metal cluster size and catalyst-to-biomass ratio. Fuel Process Technol 2018;178:251–61.
[47] Ogoshi S. Nickel Catalysis in Organic Synthesis. Wiley-VCH; 2020.
[48] Freel J, Galwey AK. Hydrocarbon cracking reactions on nickel. J Catal 1968;10:277–89.
[49] Shafizadeh F. Introduction to pyrolysis of biomass. J Anal Appl Pyrol 1982;3(4):283–305.